IOP Conf. Series: Materials Science and Engineering **229** (2017) 012034 doi:10.1088/1757-899X/229/1/012034

Mechanical, Thermal and Acoustic Properties of Open-pore Phenolic Multi-structured Cryogel

Rui Yao[1,2,*], Zhengjun Yao[1,2], Jintang Zhou[1,2], Peijiang Liu[1,2] and Yiming Lei[1,2]

[1]College of Materials and Technology, Nanjing University of Aeronautics and Astronautics, Nanjing 211100, China
[2]Jiangsu Key Laboratory of Advanced Structural Materials and Application Technology, Jiangsu, China

*277462297@qq.com

Abstract: Open-pore phenolic cryogel acoustic multi-structured plates (OCMPs) were prepared via modified sol gel polymerization and freeze-dried methods. The pore morphology, mechanical, thermal and acoustic properties of the cryogels were investigated. From the experimental results, the cryogels exhibited a porous sandwich microstructure: A nano-micron double-pore structure was observed in the core layer of the plates, and nanosized pores were observed in the inner part of the micron pores. In addtion, compared with cryogel plates with uniform-pore (OCPs), the OCMPs had lower thermal conductivities. What's more, the compressive and tensile strength of the OCMPs were much higher than those of OCPs. Finally, the OCMPs exhibited superior acoustic performances (20% solid content OCMPs performed the best) as compared with those of OCPs. Moreover, the sound insulation value and sound absorption bandwidth of OCMPs exhibited an improvement of approximately 3 and 2 times as compared with those of OCPs, respectively.

1. Introduction

Since the bonding strength, rate of carbon residue and chemical stability of phenolic resin are high, meanwhile, it has low smoke and toxic. Phenolic resin can be used as adhesive, fire insulation and anti-corrosion materials [1-3]. Among them, phenolic foams with light weight, good heat resistant and low thermal conductivity exhibit good application prospects on the fields of thermal insulating materials [4,5]. Nevertheless, the applications of traditional phenolic foam materials are limited because of their large brittleness and high powder dropping rate[6]. While phenolic cryogels which are prepared by freeze-drying method has declined the brittleness and powder dropping rate. This is mainly caused by their three-dimensional reticular structure [7,8]. In addition, the solid contents of the materials is low, which has badly blocked the heat conduction in the thermal transfer process. Moreover, due to their nano-sized holes, thermal convection and radiation are severely weakened and obstructed. The phenolic cryogel materials exhibit better thermal insulation performance under above effects [9-12].

Therefore, compared with phenolic traditional phenolic foam materials, cryogel materials own higher implementation value. In addition, the nano-sized holes of cryogel materials are mostly even with hole area percentages more than 95%. This big amount of holes offer sufficient space for sound to

shuttle and rub with the cryogel skeleton. Hence, the sound absorption ability of phenolic cryogels is excellent [13]. However, attributed to the uniform pore structures of the cryogels, the sound absorption spectra of these materials is narrow. At certain frequencies, the pores with similar size exhibit good sound absorption performance, while the absorption performance emerge significantly decreases at other frequencies [14]. To solve this issue, OCMPs were designed and prepared. The OCMPs were composed of three layers: the top and bottom of the layers owned a pyknotic structure with sectional tiny pores, while the interlayer exhibited an multi-pores structrue which owned micro-pores together with irregularly dispersed nano-pores [15,16]. Attributed to their broad size distribution, this mult-structure lead to the increase of the sound absorption spectrum width. Therefore, these materials can be used as sound absorption materials in the fields of building, vehicle, and aerospace, such as auto interior decoration, household ceiling, submarine stealthy materials and so on[17,18].

2. Experimental details

2.1. Preparation of phenolic cryogels

Phenolic cryogels were prepared by a three-step method. Phenolic hydrogels were made from resorcinol (R) and formaldehyde (F) [19], then acetic acid was used to dispose the hydrogels. After freeze-drying, phenolic cryogels were obtained [20].

First, water, sodium carbonate, formaldehyde, resorcinol were mixed uniformly (molar ratio, R: F=1: 2, Na_2CO_3: R=1: 150) and made into hydrogel plates under certain conditions (80 ℃, 1-2 h, 50KHz ultrasound). Second, the hydrogels were put into the 2wt% acetic acid solution disposing for 5 days, then they were immersed into 5wt% acetic acid solution (1 day) for further enhancement. Third, through freeze-drying at -50℃ by lyophilizer for 1 day, open-pore phenolic cryogel acoustic multi-structured plates (OCMPs) were obtained. In addition, cryogel plates with uniform-pore (OCPs) were obtained after the hydrogel plates were disposed by 5wt% acetic acid solution and 99wt% tert butyl alcohol for 5 and 7 days, respectively

For OCMPs samples A1 to A4, the solid contents of the hydrogels were 10wt%, 15wt%, 20wt% and 25wt%. Meanwhile, one OCP sample B1 were prepared with 20wt % solid contents.

2.2. Microstructures and Characterizations.

Field Emission Scanning Electron Microscopy (FESEM) was measured through S-4800 ice launch scanner (Hitachi, Japan). X-ray photo electron spectroscopy (XPS) was obtained using Thermo ESCALAB 250XI multifunctional imaging electron spectrometer (Thermo, USA). Pore analysis was tested by JW-BK132F specific surface area and pore size analyzer (Jingwei, China). Fourier Transform Infrared Spectroscopy (FTIR) was measured by PerkinElmer Spectrum 100 FT-IR Spectrometer (PerkinElmer, America). X-ray Diffraction (XRD) was measured by Bruker D8 Advance Eco (Bruker, Germany).

2.3. Mechanical testing

A CMT5105 electronic universal testing machine was used to test the composites' compression and tensile performances. To produce an average and variance, five replicates were applied in the mechanical tests.

2.4. Thermal testing

Perkin-Elmer Pyrisl calorimeter and DSC-2 thermal analyzer were used to proceed TG-DSC analysis. The temperatures were ranged from 30 to 850℃ with 10℃/min heat increasing rate under N_2 atmosphere.

Thermal conductivities of the plates were measured by a Hot Disk TechmaxTPS1500 thermal meter (Sweden).

2.5. Acoustic testing

Impedance Measurement Tube for ASTM Type 4206A, Pules Multi-analyzer system Type 3560 and Power Amplifier Type 2716 (B&K, Denmark) were used to evaluate transmission loss and absorption coefficient.

3. Results and discussion

3.1. Pore mophology and size analysis of the aerogels.

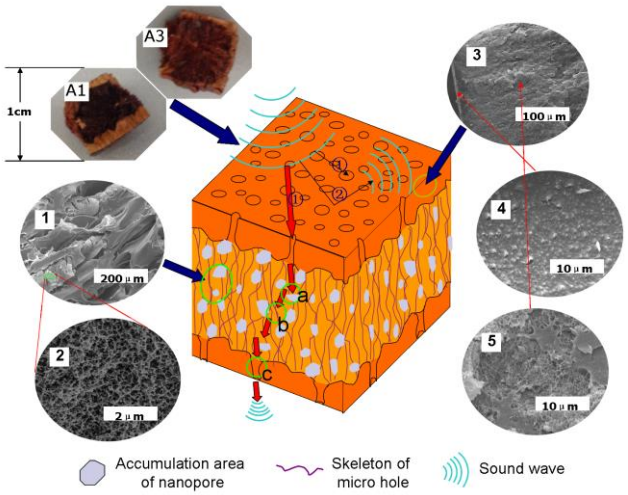

Figure 1. The photographs of the actual products A1 and A3, as well as the SEM images of A3 and the simulated diagram and sound transmission mechanism of OCMP samples.

The photographs of the actual samples A1 and A3, as well as the SEM images of sample A3 and the simulated diagram of OCMPs' sound transmission mechanism are illustrated in Figure 1. Seen from the photographs, the boundary walls of sample A3 were thinner than those of A1. The OCMPs exhibited a porous sandwich structure, which can be viewed from the SEM images. Through further observation, the specific structure of the cryogels were as follows. The morphology of the boundary walls were displayed in the SEM images '3, 4, and 5'. They showed a poriferous surface and a relatively dense structure compared with the center section. While the structure of the interlayer contained micro-holes with randomly dispersed nano-pores on their inner part, which was exhibited in the SEM images '1 and 2' [21]. The formation mechanism of the sandwich microstructure is explained through the simulated diagram. The SEM image '2' has roughly assumed the skeletons of the hydrogels, however, when freeze-dried, the skeletons of the hydrogels are partly destroyed by the surface tension of water under pumpdown action, which emerges from the center to the surface. As a consequence, thick boundary walls are formed by the agglomerated materials which spread from the cracked skeleton. Meanwhile, the nano-pores has fused together, which lead to the development of micro holes in most part of the interlayer region, however, there still maintain nano-pores in other areas. The skeleton of A3 which own higher solid content is stronger than A1, hence, it's more difficult for A3 to destroy its interlayer by the surface tension of water than A1. In addition, the boundary walls will become thnner with the decrease of the cracked skeleton materials. Eventually, with the help of the images of the actual samples and the microstructure, a simulated diagram of OCMPs' sound transmission mechanism was constructed in Figure 1, and the mechanism will be elaborated below.

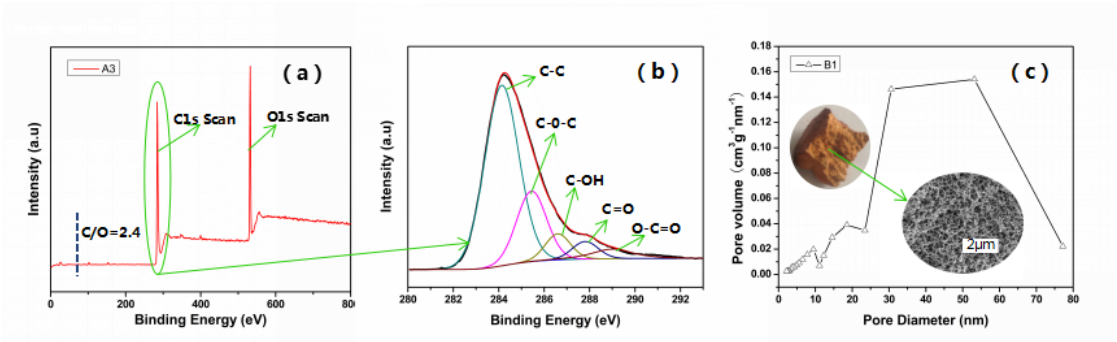

Figure 2. XPS measurements of A3, as well as the morphology, macroscopic pattern, and pore size desorption of sample B1.

XPS curves of A3, as well as the morphology, photograph, and pore size desorption (BJH method) of sample B1 are displayed in Figure 2. In Figure 2a, around 286 and 533 eV, two peaks appeared, which is attributed to C and O elements, respectively. The atomic ratio of carbon and oxygen (C/O ratio) was 2.4, and it's in accordance with the range of theoretical ratio which was between 2 and 4 according to chemical dehydration-condensation reaction (R:F=0.5), in the other hand, this result stated that the cryogels had complex chemical bonds. In addition, observed from the peaks caused by C–O–C and C=O groups in Figure 2b, the same conclusion was obtained. Simultaneously, there exised characteristic peaks attributed to C–C, C–OH and O-C=O groups, while the peak of C–C groups also contained methylene bonds [22]. Seen from Figure 2c, the pore diameters of sample B1 were mostly ranged from 30 nm to 50 nm. In addition, the nano-pores of sample B1 exhibited almost the same size as that of sample A3. OCMPs has similar nano-pores structure as OCPs, albeit they have quite different macroscopic patterns.

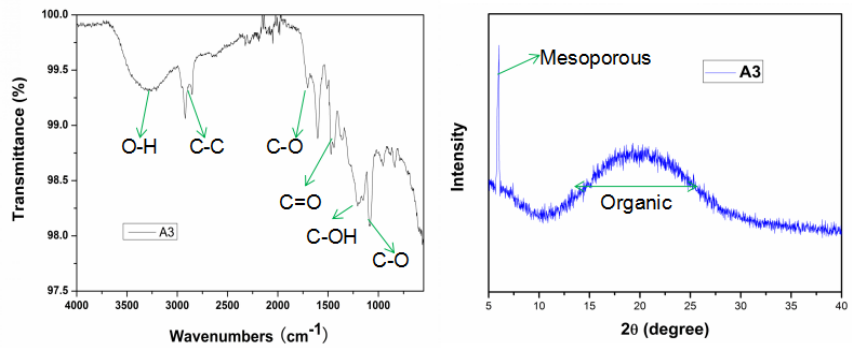

Figure 3. FTIR and XRD curves of A3.

Seen from the FTIR image (left image of Figure 3), RF cryogels show the similar groups as XPS image. Viewed from the peaks of FTIR image, there existed O-H, C-C, C-O, C=O and C-OH groups in the cryogels. Through above analysis, it's obvious that RF cryogels were obtained successfully.

In XRD curves (right image of Figure 3), RF cryogels emerge broad peaks, which is attributed to that they are organic materials. In addition, there existed poignant peaks on the curve of the cryogels at the small angle, indicating that there were mesoporous inside these cryogels, which was consistent with the result of the Figure 2c.

3.2. Mechanical and thermal properties of the aerogels

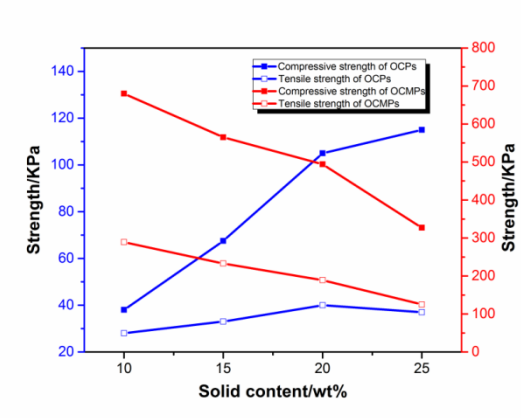

Figure 4. Compressive and tensile strength of OCPs and OCMPs.

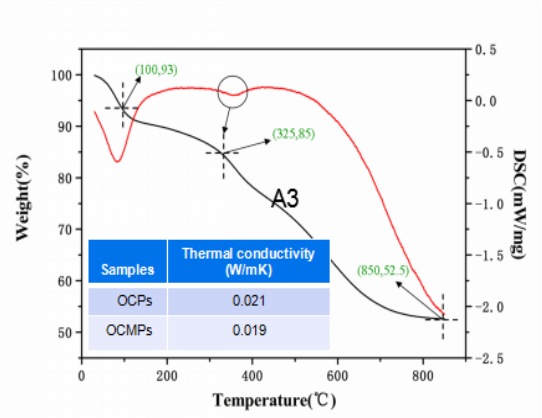

Figure 5. TG-DSC curves of A3 as well as thermal conductivity of OCPs and OCMPs

The compressive and tensile strength of the cryogels are shown in Figure 4. When the solid content reaches 10 wt.%, the compression and tensile strength of OCMPs reached their maximum. After that, they began to decrease significantly. While OCPs exhibited the opposite results. They were the minimum at the 10 wt.% solid content, then gradually increased. For OCPs, since they were uniform structure, the increase of the solid content will surely increase the structure strength, lead to the increase of their compressive and tensile strength. But for OCMPs, the mainly bearing part was the boundary walls, they became thin with the increase of solid content concluded from above results. So their strength will surely decrease. In addition, compared with the strength of OCPs, the compressive strength and tensile strength of OCMPs are much higher, which is also caused by the boundary walls.

Figure 5 displays the TG-DSC curves of sample A3. Three key points of the sample were marked in the TG-DSC curves. Since the specific surface area and porosity of cryogels were large, the water vapor in the air was absorbed into the pores. When the temperature reached 100 ℃, the absorbed water was evaporated which made 7% weight lost of the sample, and this was the first key point. After that, the second key point will appear at 325 ℃ with 15% weight lost of the sample. At this temperature, the sample will be decomposed acutely. Accordingly, in the DSC curve, an exothermic peak will emerge. Finally, the third point was found at the temperature of 850 ℃, and the weight lost of the sample become invariant at 47.5%, and this stability was caused by the C element (The groups of H and O elements were completely broken and wiped off, while C element maintained under higher heat resistance). Generally speaking, the cryogel materials had high thermal resistance, and they will become carbon cryogels with higher thermal resistance.

The thermal conductivities of cryogel samples under normal temperature are tested and showed in the table of Figure 5. Viewed from the table, the thermal conductivity of OCMPs was higher than that of OCPs, which was mainly attributed to the block action of the close-grained boundary walls to the thermal convection.

3.3. Acoustic properties of the aerogels as well as sound absorption and insulation mechanism

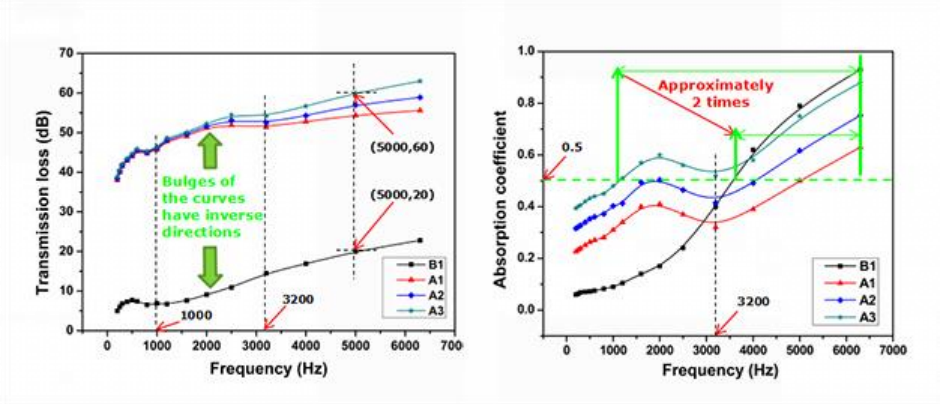

Figure 6. The transmission loss and sound absorption coefficient of OCMP and B1 samples.

Figure 6 shows the sound performances of OCMPs and B1 samples. Sample A4 was excluded from the test for its agglomeration. The transmission loss of B1 increased quickly at first with the increase of frequency, then the growth speed lowed down. For sound absorption coefficient, it was the same trend. In addition, the sound performances of OCMPs exhibited similar trends as those of B1. Samples A3 and B1 have same ingredient and solid content, while they have a biggest difference which reflects in their structures. B1 has an uniform nanopores structure, while A3 has solid boundary walls at two surfaces with inner micro pores and nanopores. The solid boundary walls which obstruct the sound waves make the TL value of A3 much higher than that of B1. But for sound absorption coefficient, the boundary walls make less sound waves be consumed by the inner pores which in turn leads to the decline of sound absorption. At the same time, the boundary walls have through-holes which reduce barrier effects and enhance consumption of sound waves. In view of the comprehensive function of above two aspects, these two samples present similar sound absorption coefficients.

Nevertheless, from 1000 Hz to 3000 Hz, there occurred a significant difference: Compared with other frequencies, the sound performances showed great improvement. In general, compared the transmission loss of A3 with that of B1 at 5000 Hz, the improvement was almost 3 times. Meanwhile, compared the samples A1, A2 and A3, it is concluded that the sound absorption coefficient will increasingly improve with the increase of solid content. The primary sound insulation mechanism is elaborated in the simulated diagram of Figure 1: As shown in Figure 1, a sound wave transmits into the surface and interior of OCMPs, it will become three waves: absorbed, reflected, and transmitted wave. The boundary walls is the significant factor to form the reflected wave. After reflection, the remained wave is running along path 1. Then, the sound will rub with the medium (Figure 1“a,b,c”), the sound wave which is consumed here is the absorbed wave. After absorption and reflection of the materials, The sound wave that survives is the transmitted wave. Under this sound insulation mechanism, the sandwich structured OCMPs guarantee sound waves to spread and consume with the surface and interior of the materials adequately. In addition, when the absorption coefficient exceeds 0.5, the absorption frequency spectrum of OCMPs and OCPs have improved about 2 times. The solid content of sample A3 is the highest compared with other samples, so its skeleton structure is compact which can absorb more sound energy. This will surely make sample A3 exhibit the best sound performance. However, with the increase of solid content, the boundary walls will become thinner, which will decline the transmission loss in some degree [23].Through above analysis, the 20% solid content OCMPs have presented the best sound performance.

4. Conclusions

In this study, a type of a sandwich-like multi-structure was designed for obtaining better acoustic performance. Afterwards, the OCMPs were observed to have been manufactured into this type of structure through microscopic morphology. In addtion, compared with cryogel plates with uniform-pore (OCPs), the OCMPs had lower thermal conductivities. What’s more, the compressive and tensile strength of the OCMPs were much higher than those of OCPs. Finally, The OCMPs

exhibited superior acoustic performance (20% solid content OCMPs performed the best) as compared with that of OCPs. Moreover, the sound insulation value and sound absorption bandwidth of OCMPs exhibited an improvement of approximately 3 and 2 times as compared with those of OCPs, respectively.

Acknowledgements
This work is supported by the Opening Project of Jiangsu Key Laboratory of Advanced Structural Materials and Application Technology (PAPD). as well as National Natural Science Foundation of China (Funding NO. 51672129)

References

[1] A. Tadaharu, K. Takao and H. Masahiro, International Journal of Adhesion and Adhesives , 53 , 53 (2015).
[2] X.Y Sui and Z.Z Wang, Polymers for Advanced Technologies , 24 , 593 (2013).
[3] K. Guo, X.G. Li, Z.W. Yue, X.G. Wang, F.J. Yan, X.M. Wang, Jianmei Gao and Zhibin Fan, Polymer composites , 36 , 1346 (2015).
[4] Y. Wang, S.J. Wang, C. Bian, Y.H. Zhong and X.L. Jing, Polymer Degradation and Stability , 111 , 239 (2015).
[5] L.P. Bian, J.Y. Xiao, J.C. Zeng, S.L. Xing, C.P. Yin and A.Q. Jia, Materials & Design , 54 , 230 (2014).
[6] U.A. Amran, S. Zakaria, C.H. Chia, S.N.S. Jaafar and R. Roslan, Industrial Crops and Products, 72 , 54 (2015).
[7] R. Zhang, Y.G. Lu, L. Zhan, X.Y. Liang, G.P. Wu and L.C. Ling, Carbon , 41 , 1660 (2003).
[8] L.I. Grishechko, G. Amaral-Labat, A. Szczurek, V. Fierro, B.N. Kuznetsov and A. Celzard, Microporous and Mesoporous Materials, 168 , 19 (2013).
[9] T.A. El-Brolossy, S.S. Ibrahim and E.A. Alkhudhayr, Polymer Composites, 36 , 1242 (2014).
[10] E. Cuce, P.M. Cuce, C.J. Wood and S.B. Riffat, Renewable and Sustainable Energy Reviews, 34 , 273 (2014).
[11] R.J. Goldstein, E.R.G. Eckert, W.E. Ibele, S.V. Patankar, T.W. Simon, T.H. Kuehn, P.J. Strykowski, K.K. Tamma, A. Bar-Cohen, J.V.R. Heberlein, J.H. Davidson, J. Bischof, F.A. Kulacki, U. Kortshagen, S. Garrick and V. Srinivasan, International Journal of Heat and Mass Transfer, 48 , 819 (2005).
[12] E.M. Sparrow, S.S. Kang and W. Chuck, International Journal of Heat and Mass Transfer, 30 , 1237 (1987).
[13] G.P. Wu, J.B. Yang, D.P. Wang, R. Xu, K. Amine, C.X. Lu, Mater Lett, 115 , 1 (2014).
[14] G.Q. Tang, Z.G. Jiang, X.F. Li, H.B. Zhang, D. Aravind, Carbon, 77 , 592 (2014).
[15] W.F. Chen, S.R. Li, C.H. Chen, L.F. Yan, Adv Mater, 23 , 5679 (2011).
[16] X. Xu, H. Li, Q.Q. Zhang, H. Hu, Z.B. Zhao, J.H. Li, et al, ACS Nano, 9 , 3969 (2015).
[17] J.Z. Feng, J. Feng, Y.G. Jiang, C.R. Zhang, Mater Lett, 65 , 3454 (2011).
[18] R. Baetens, B.P. Jelle, A. Gustavsen, Energ Buildings, 43 , 761 (2011).
[19] H. Reuter, Adv Mater, 3 , 568 (1991).
[20] F. He, C. Sui, X.D. He, M.W. Li, Mater Lett, 152 , 9 (2015).
[21] T. Zhu, K.Y. Teng, J. Shi, L. Chen, Z.W. X, Compos Sci Technol, 123 , 276 (2016).
[22] Q.Y. Peng, Y.B. Li, X.D. He, X.C. Gui, Y.Y. Shang, Adv Mater, 26 , 3241 (2014).
[23] P.S. Allan, A. Ahmadnia, R. Withnall, Polym Test, 31 , 312 (2012).